EFFECT OF FINITE BARYON DENSITY IN FREE ENERGY CALCULATION UNDER ONE-LOOP CORRECTION

S. Somorendro Singh[*1]

[1]*Department of Physics and Astrophysics, University of Delhi, Delhi - 110007, India*

[*]Corresponding Author: sssingh@physics.du.ac.in

(Received 19 September 2025; revised 10 March 2026; accepted 27 March 2026; published 1 August 2026)

Abstract: The free energy evaluation is studied under one-loop correction at finite baryon density. The finite baryon density in this one-loop correction results in bubble/droplet formation achieved with quark and gluon parametrization in the range of $\gamma_q = 1/8$ and $8\gamma_q \leq \gamma_g \leq 18\gamma_q$. Stable droplets are specifically realized when the quark and gluon parameterizations satisfy $\gamma_q = 1/8$ and $12\gamma_q \leq \gamma_g \leq 16\gamma_q$. So this baryon density enhances the stability of the droplets of quark-gluon plasma (QGP) with a smaller size. This implies that incorporating finite baryon density into the free energy calculations provides significant insights into QGP formation. Therefore, the model with one-loop correction at finite baryon density is suitable for describing QGP signals.

Keywords: Quark-gluon Plasma; Quark-Hadron phase transition; Quantum chromodynamics; Free energy

PACS: 12.38 Mh; 12.29 Pn; 25.75Ld

1 Introduction

The strong interaction theory called ”Quantum Chromodynamics” (QCD) can describe characteristic features of coloured quarks and gluons. QCD frameworks predict a distinct phase transition where these colored, unconfined quarks and gluons condense into color-neutral bound states known as hadrons. [1, 2]. This change of nature is believed to occur under extreme conditions of high nuclear density or very high temperature. So, the matter formed in these two extreme conditions is designated as the quark-gluon plasma (QGP). Because QGP states are highly transient and short-lived, tracking and predicting their behavior remains a complex task. Nevertheless, investigating such challenging phenomena is a common pursuit to uncover their inner nature. So, the topic is a burning candidate for investigation of these phases. Globally, several specialized experimental centers study these phases, notably the Relativistic Heavy-Ion Collider (RHIC) at BNL and the Large Hadron Collider (LHC) at CERN. Complementing these major operations, newer research facilities like FAIR at Darmstadt and NICA at Dubna are explicitly configured to explore physics at compact baryon densities [7, 8]. These specialized laboratories prioritize the investigation of dense baryonic matter. For instance, Baryonic Matter at Nuclotron (BM@N) experiments utilize high-energy ion beams from the Nuclotron to recreate particle production conditions mirroring the early universe's evolution. Again, from lattice's point, there is report of involving the finite baryon density in the study of QGP formation [9, 10]. However, the facilities available to these experiments will also provide the detailed news of the early universe phase transition, quark-gluon plasma droplet formation, and phase structure picture of QCD [11–14].As a result, modeling QGP within ultra-relativistic heavy-ion collisions stands out as a frontier area in modern collider physics , drawing intense interest from theorists and experimentalists seeking to leverage baryon density as a key dynamical variable. QGP signatures are expected to manifest near the convergence of high baryonic density and temperature, where both distinct phases coexist [15, 16]. There is also information about QGP formation at the convergence of baryonic density and temperature, where both phases exist [17]. In this short paper, the calculation of free energy evolution is concentrated with the effect of finite baryon density under the purview of one-loop corrections. The underlying baryon density is directly determined by the total population of charged particles within the thermodynamic system. Given contemporary paradigms of

QGP evolution, the presence of these finite baryon densities cannot be disregarded. It has been experimentally observed that the high-speed particles are the charged particles. Based on this information, laboratories like CBM (compact baryon matter) in Darmstadt, Germany are established for the detail study about these charged particles. So, the consideration of finite baryon density in the present calculation is reasonable in the context of phenomenological studies. To determine the free energy, we construct a thermodynamic partition function that establishes a link between Gibbs free energy and finite baryonic density. The one-loop corrected partition function within the mean-field potential framework is adjusted by redefining the density of states to accommodate baryonic density factors. This modified density of states is formulated via dynamic quark and gluon flow parameters, where the effective quark masses are shifted by both the baryon density and loop corrections. Consequently, the free energy expansion of the expanding QGP fireball varies with the quark and gluon flow parameters, modifying droplet stability across different flow conditions [18–20]. These flow parameters are critical in determining how stable droplets or bubbles develop as the system's temperature rises. Again, one of the most successful model to explain about the description of QGP formation is the relativistic hydrodynamics, which provides the quantitative pictures of heavy-ion collision dynamics [21–23] However, the hydrodynamic approach tends to yield next generation approximations for better model- data agreement [24, 25].

Briefly, the density of states at finite baryon density is restudied and next evaluate the free energy computing the free energy evolution by incorporating one-loop effects alongside the quark and gluon flow parameters. In the evaluation, the quark mass is considered with temperature and baryon density dependence. So the temperature is taken in such a way that QGP-phase transition is normally observed during temperature $(150 - 270)$ MeV and due to it, the bubble/droplet formation is observed within the range of these temperatures. However, the baryon density is considered on a random choice with the scale of temperature at which the appropriate value of the baryon density may be achieved. Now we look at the changes in the free energy produced by this.

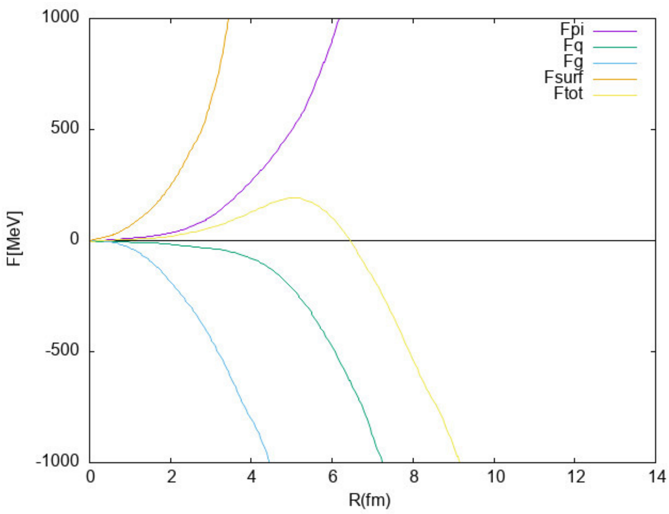

Figure 1: Free energy graph of individual particles vs. R at $\gamma_q = 1/8$, $\gamma_g = 12\gamma_q$ for particular temperature $T = 170\ MeV$ and baryonic chemical potential $\mu_B = \mu/3$ where, $\mu = 300$ MeV.

2 Density of state with one-loop correction at finite baryon density

The density of states of the present calculation is obtained through the potential model. The interacting potential defined at this finite baryonic density is obtained through the extension of earlier one-loop correction potential [26–28]. However, the idea of potential interaction is brought from the static potential to dynamical quarks as it has a finite value depending on the temperature, which can play a little role in influencing the potential between quarks and anti-quarks. While the static potential originates from heavy quark masses and the system is under the influence of high and baryonic density. Due to it, the dynamic quark mass is perturbed by high temperature and chemical potential. So its value has been compared to the heavy quark mass and the interaction potential of these

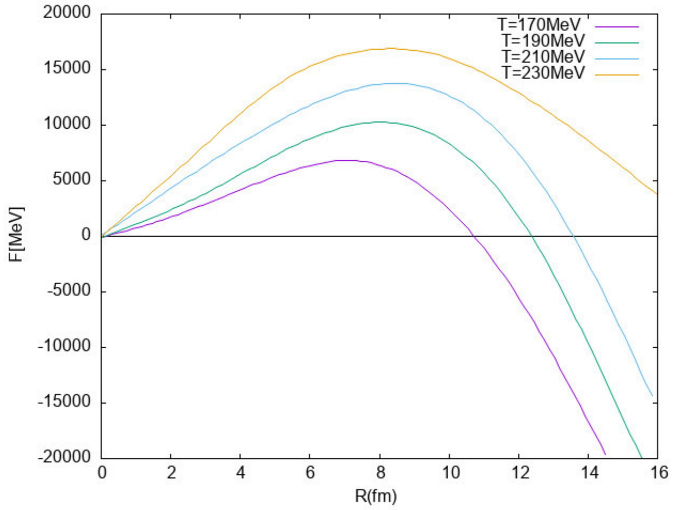

Figure 2: Total free energy versus R the size of the droplet at $\gamma_q = 1/8$, $\gamma_g = 8\gamma_q$ and $\mu_B = \mu/3$ where, $\mu = 300\ MeV$ for various temperatures.

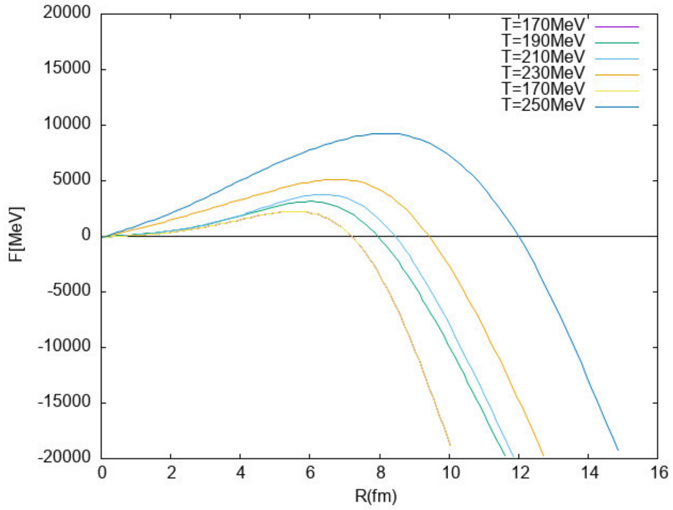

Figure 3: Total free energy versus R the size of the droplet at $\gamma_q = 1/8$, $\gamma_g = 10\gamma_q$ and$\mu_B = \mu/3$ where, $\mu = 300\ MeV$ for various temperatures.

modified quark masses has been obtained. It is now expressed as:

$$V(p,\mu) = \frac{8\pi}{p}\gamma\alpha_s(p,\mu)(T^2+\mu^2/\pi^2)[1+\frac{\alpha_s(p,\mu)}{4\pi}b_1] - \frac{m_0^2}{2p} \tag{1}$$

where γ represents the RMS (root mean square) value of the quark and gluon flow parameters say $\gamma_q = 1/8$ and $\gamma_g = (8-16)\gamma_q$. $\alpha_s(p,\mu)$ is defined as done in earlier papers. It is:
$\alpha_s(p,\mu) = \frac{4\pi}{29\ln[1+(p^2+\mu^2)/\Lambda^2]}$ in which Λ is the quantum chromodynamics parameter normally taken as $150\ MeV$. μ is taken in terms of baryon chemical potential as $\mu = 3\mu_B$, μ_B is finite baryon chemical potential. b_1 is the one-loop correction factor, which is defined as

$$b_1 = 2.5833 - 0.2778n_l \tag{2}$$

where n_l is light quark numbers of flavor $2+1$ as u,d and s [29, 30]. So using this potential we obtain the density of state as:

$$\rho(p) = \frac{v}{\pi^2}[\frac{\gamma^3(T^2+\mu^2/\pi^2)}{2}]^3 g^6(p)A \tag{3}$$

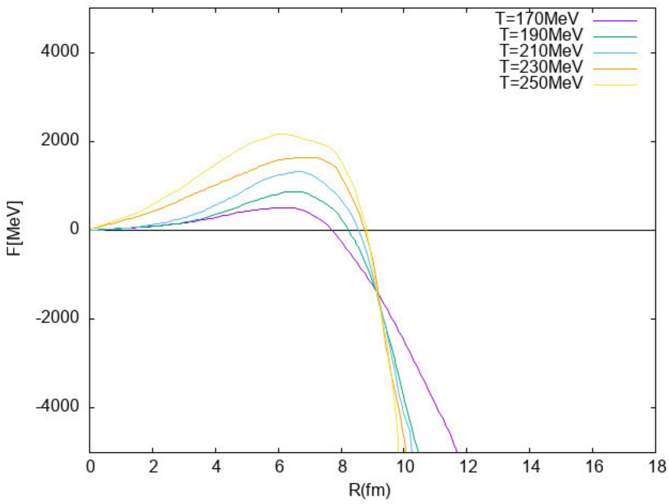

Figure 4: Total free energy vs. R the size of the droplet at $\gamma_q = 1/8$, $\gamma_g = 12\gamma_q$ and $\mu_B = \mu/3$ where, $\mu = 300\ MeV$ for different temperatures.

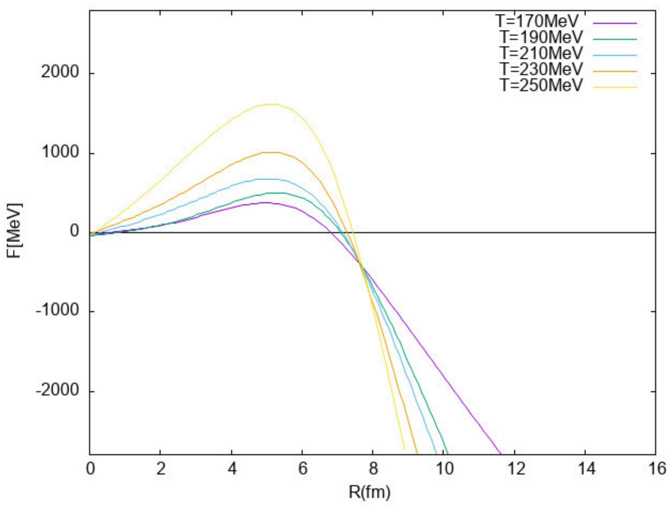

Figure 5: Total free energy vs. R the size of the droplet at $\gamma_q = 1/8$, $\gamma_g = 14\gamma_q$ and $\mu_B = \mu/3$ where, $\mu = 300\ MeV$ for various temperatures.

Eq. (3) defines the modified density of states in phase space, revised to incorporate one-loop corrections within an interacting potential at a finite baryonic chemical potential μ_B. It is really obtained through reviewing our earlier paper on one-loop corrections. In the expression, v is the QGP occupied volume. $g^2(p) = 4\pi\alpha_s(p, \mu)$ and A is a factor of one-loop coupling constant obtained in simplifying the density of state through the potential in the above expression (1). It is found as:

$$A = \{1 + \frac{\alpha_s(p, \mu)b_1}{\pi}\}^2 [\frac{(1 + \alpha_s(p, \mu)b_1/\pi)}{p^4} + \frac{2(1 + 2\alpha_s(p, \mu)b_1/\pi)}{p^2(p^2 + \Lambda^2)\ln(1 + \frac{p^2+\mu^2}{\Lambda^2})}] \tag{4}$$

3 Thermodynamic free energy at finite baryon density

The relevant thermodynamic potential can be constructed by knowing the temperature, the finite baryon density and the Hamiltonian of the system. So the partition function of the system is defined in a number of literature is as [31]

$$Z(T, \mu, V) = Tr\{exp[-\beta(\hat{H} - \mu\hat{N})]\} \tag{5}$$

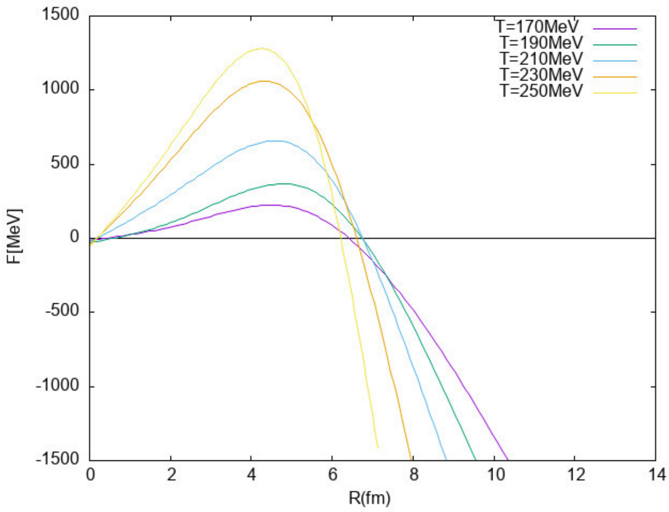

Figure 6: Total free energy vs. R the size of the droplet at $\gamma_q = 1/8$, $\gamma_g = 16\gamma_q$ and $\mu_B = \mu/3$ where, $\mu = 300\ MeV$ for various temperatures.

where $\beta = \frac{1}{T}$, μ represents the chemical potential expressed relative to the baryon chemical potential ($\mu = 3\mu_B$), $\hat{N}$ denotes the quark number operator, and T is the temperature. Now it is co-related the Gibbs free energy using the partition function. It is related in this way as [32–34]:

$$F_i = T \ln Z(T, \mu, V) \tag{6}$$

The free energy evolution is subsequently established by integrating the density of states with the appropriate Fermi-Dirac and Bose-Einstein distribution functions for fermions and bosons, respectively:

$$F_i = \pm T g_i \int \rho_{q,g}(p) \ln[1 \mp e^{-(\sqrt{m_i^2+p^2}-\mu)/T}] dp \ , \tag{7}$$

In this formulation, the quark mass depends explicitly on both temperature and finite baryon density. The term g_i accounts for the degeneracy factors associated with color and particle-antiparticle degrees of freedom for quarks and gluons. The term $\rho_{q,g}$ denotes the phase-space density of states modified by one-loop corrections within the interaction potential at baryon density μ_B. Integrating these factors across the free energies of fermions and bosons allows us to map the dynamics of the QGP flow. In addition to these bulk free energies, we incorporate an interfacial energy term to account for hydrodynamic movements within the medium, alongside a Bag energy constant to enforce confinement. This surface term is also evaluated using the root mean square flow parameters of quarks and gluons: [35, 36].

$$F_{interface} = \frac{\gamma T R^2}{4} \int p^2 \delta(p - T) dp, \tag{8}$$

In the above equation, γ is already defined in eq. (1) This parameter controls the QGP fluid dynamics and is introduced when interfacial energy forms to counterbalance the bag energy pressure, where R signifies the radius of the QGP droplet. To account for the hadronic phase, the free energy contributions from medium-mass hadrons (which dominate the reaction zone with degeneracy factor g) are given by: [37]:

$$F_h = (gT/2\pi^2)\nu \int_0^\infty p^2 \ln[1 - e^{-(\sqrt{m_h^2+p^2}-\mu/T)}] dp. \tag{9}$$

where m_h represents the mass of the corresponding hadronic species. These hadrons are considered to be medium-mass hadrons as they are the dominant factor in the reaction zone. Finally, all these contributed free energies are added and then the total modified free energy F_{total} is computed as:

$$F_{total} = \sum_i F_i \ + \ F_{interface} \ + \ F_h, \tag{10}$$

where index i runs over u, d, s quarks, and gluons.

4 Results

This section presents numerical solutions to the free energy expressions derived from our potential-based density-of-states model. The Fig. 1 demonstrates the free energies of the individual participants e.g quarks, gluons, interfacial, the most dominant contribution pions among the hadrons. So the corresponding plots of the individual particles present in the figure show the energy evolution carried by these particles. Then the figure is traced at the choice of baryonic chemical potential $\mu_B = \mu/3$ where, $\mu = 300\ MeV$ and at temperature $T = 170\ MeV$. This temperature is generally taken as the transition temperature. Then it tries to represent the free energy summing up all the contributions of the involved particles together in this Fig. 1. However, in considering all the particles among hadrons, it is taken only few of particles having less masses than $1000\ MeV$ of hadrons as these masses contributed somewhat more in comparison to other massive hadrons in the reaction zone. So the Fig. 2 is plotted for all these contributed particles of hadrons, quarks, gluon and interface. This combined free energies indicate the droplet formation of different sizes according to the different temperatures at quark and gluon parameters $\gamma_q = 1/8$ and $\gamma_g = 8\gamma_q$. At this particular parameter the droplets are formed at the different temperatures and there is no stability in the droplet of QGP bubbles. With the increasing temperature, the size of the droplet increases at this finite baryonic chemical potential with the same flow parameter.

Again, in Fig. 3, the free energy vs the size of droplet is plotted at the quark flow parameter fixed at $\gamma_q = 1/8$ and increased gluon flow parameter to $\gamma_g = 10\gamma_q$. At such a parameter the droplets/bubbles are found but they are still unstable droplet at this baryon chemical potential $\mu_B = \mu/3$ with $\mu = 300\ MeV$ with smaller sizes. It indicates that the droplet size is still visible in obtaining smaller droplets with the fixed quark and increased gluon flow parameters. Then it is further searched to find suitable stable droplets of QGP with an ad-hoc search of gluon parameters in Fig. 4 to 6. In these figures, the stable droplets are able to find at a slight different value of gluon flow parameter. In Fig.4 the stable droplet is seen with the size of the droplet around $9\ fm$ at $\gamma_q = 1/8$ and $\gamma_g = 12\gamma_q$. It indicates that there is stable drop of QGP if there is a suitable choice of the gluon flow parameter. Again in Fig.5 the same situation is obtained with slightly changed in the size of droplets. The size is found to be around $8\ fm$ with the marginal change of the gluon flow parameter at $\gamma_g = 14\gamma_q$. It shows that the droplet is more stable with the increase of temperature with increased gluon parameter. In Fig.6, the gluon flow parameter is increased a little and there is a slight change in the stability of the droplet. It implies that the stable droplets are not able to obtain for any range of gluon flow parameter beyond this value, $\gamma_g = 14\gamma_q$. It says that the stable/unstable droplets are obtained in a particular range of the gluon parameter say $\gamma_q = 1/8$ and $12\gamma_q \le \gamma_g \le 16\gamma_q$ Beyond this window, the QGP droplet dynamics become highly turbulent across variations in temperature and chemical potential. Stable fluid configurations are strictly locked within the narrow range of $12\gamma_q \le \gamma_g \le 14\gamma_q$. This localized stability stems from the temperature and chemical potential dependence embedded in the quark masses via the one-loop corrected potential model. Hence, incorporating a baryonic chemical potential alongside one-loop corrections is capable of generating stable, equilibrium droplets in QGP flow profiles.

Therefore, as a final remark, a one-loop correction considering a baryonic chemical potential can generate an equilibrium/stable droplet in the flow dynamics of QGP.

To summarize, by building upon our established one-loop calculations and introducing a finite baryonic chemical potential, we have shown that stable droplet configurations remain a viable outcome in QGP hydrodynamics.

5 Conclusion

We have demonstrated that the simultaneous inclusion of a finite baryonic chemical potential and one-loop corrections to the mean-field potential leads to distinct windows of stability and instability in droplet formation. These states are sensitive to the chosen quark and gluon flow parameters, spanning the range $\gamma_q = 1/8$ and $12\gamma_q \le \gamma_g \le 16\gamma_q$. In particular, robust equilibrium stability is achieved when $12\gamma_q \le \gamma_g \le 14\gamma_q$, with the resulting droplet sizes showing an expansion relative to models using uncorrected potentials. Therefore, we conclude that hydrodynamical parameters like the quark and gluon flow parameters act as critical regulatory agents controlling QGP fluid dynamics to permit stable droplet configurations. Establishing this droplet stability opens up pathways to systematically investigate other thermodynamic characteristics of the QGP medium.

Acknowledgments

The author expresses sincere gratitude to K K Gupta for insightful discussions and a meticulous reading of the manuscript. The author also thanks Tushar Bhalla for his help in preparing the figures. Finally, the author gratefully acknowledges the Institution of Eminence, University of Delhi, Delhi, for providing financial support through a faculty research program grant (Ref. No./IOE/2024/12/FRP).

References

[1] A. Ali Khan *et al.* (CP-PACS), Phys. Rev. D **63**, 034502 (2001).

[2] E. Karsch, A. Peikert and E. Laermann, Nucl. Phys. B **605**, 579 (2001).

[3] C Leticia *et al.*, Prog. Part. Nucl. Phys. **124**, (2022).

[4] E. Shinlchi, AIP Conf. Proc. **1235**, 179 (2010).

[5] Y. Akiba, Prog. Theor. Phys. Suppl, **187**, 55 (2011).

[6] P. Moreau *et al.*, Astron. Nachr, **342** 715 (2021).

[7] M. Nahrgang, J. Phys: Conf. Ser, **503**, 012001 (2014).

[8] A. Sorin *et al.*, Proc. Sc (**CPOD2014**), **217**, 042 (2014).

[9] S. Borsanyi *et al.*, Phys. Rev Lett.,**125** 052001 (2020).

[10] D. Behera, S. Deb, C. R. Singh and R, Sahoo Phys. Rev. C, **109** 014902 (2024).

[11] I. Arsene *et al.* (BRAHMS), Nucl. Phys. A **757**, 1 (2005).

[12] B. B. Back *et al.* (PHOBOS), Nucl. Phys A **757**, 28 (2005).

[13] J. Adams *et al.* (STAR), Nucl. Phys. A **757**, 102 (2005).

[14] K. Adcox *et al.* (PHENIX), Nucl. Phys. A **757**, 184 (2005).

[15] J. Randrup and J Cleymans, Eur. Phys. J. A, **52**, 218 (2016).

[16] P. Senger, Particles, **2**, 499 (2019).

[17] J. J. B-Bohr, I. N. Mishustin and Th. Dossing, Nucl. Phys. A, **923**,19 (2014).

[18] I. Nalima *et al.*, Phys. Rev D **113** , 074035 (2026).

[19] A. Peshier, B. Kämpfer, O. P. Pavlenko and G. Soff, Phys. Lett. B **337**, 235 (1994).

[20] V. Goloviznin and H. Satz, Z. Phys. C - Particles and Fields **57**, 671 (1993).

[21] Ch. Chiu and Ch. Shen, Phys. Rev. C, **103**, 064901 (2021).

[22] P Romatschke, Int. J. Mod. Phys E, **19**, 1 (2010).

[23] C. Gale, S. Jeon and B. Schenke, Int. J. Mod. Phys. A, **28**, 1340011 (2013).

[24] G. Torrieri and I. Mishustin, Phys. Rev C, **78**, 021901R (2008).

[25] T. Hirano and K. Tsuda, Nucl. Phys. A **715**, 821c (2003).

[26] W. Fischler, Nucl. Phys. B **129**, 157 (1977).

[27] A. Billoire, Phys. Lett B **92**, 343 (1980).

[28] S. S. Singh and R. Ramanathan, Prog. Theo. Expt. Phys. **2014**, 103D02 (2014)

[29] A. V. Smirnov, V. A. Smirnov and M. Steinhauser, Phys. Lett. B **668**, 293 (2008).

[30] A. V. Smirnov, V. A. Smirnov and M. Steinhauser, Phys. Rev. Lett. **104**, 112002 (2010).

[31] H. Satz, Ann. Rev. Nucl. Part. Sci. **35** 245 (1985).

[32] G. Neergaad and J. Madsen, Phys. Rev. D **60**, 054011 (1999).

[33] M. B. Christiansen and J. Madsen, J. Phys. G **23**, 2039 (1997).

[34] S. S. Singh, D. S. Gosain, Y. Kumar and A. K. Jha, Pramana J. Phys. **74**, 27 (2010).

[35] R. Ramanathan, Y. K. Mathur, K. K. Gupta and A. K. Jha, Phys. Rev. C **70**, 027903 (2004).

[36] S. S. Singh, K. K. Gupta and A. K. Jha, Int. J. Mod. Phys. A **29**, 1450097 (2014).

[37] R. Balian and C. Block, Ann. Phys. **60**, 401 (1970).